Deep Learning Object Detection for Mapping Cave Candidates on Mars: Building Up the Mars Global Cave Candidate Catalog (MGC^3)

G. Nodjoumi {1}, R. Pozzobon {2}, A.P. Rossi {1}

1} Jacobs University Bremen, Bremen, Germany, g.nodjoumi@jacobs-university.de; 2 }Department of Geosciences, University of Padova, Padova, Italy

PRESENTED AT:

INTRODUCTION

The Mars Global Cave Candidate Catalog (MGC3) v1, published by Cushing et al. [1] in 2017 contains the locations and a short description of more than 1000 possible cave-entrances on Mars that have been identified by manually surveying images acquired by Mars Odyssey's (MO) Thermal Emission Imaging System (THEMIS) and Mars Reconnaissance Orbiter's (MRO) Context Camera (CTX) and High Resolution Imaging Science Experiment (HiRISE) cameras. Authors analysed all images that covers the area north of Arsia Mons (235° to 243° E, 28° to 2° N).

The Arsia Mons is a shield volcano, located in the southern area of the large Tharsis Region, on whose flanks have been identified at least 7 possible cave entrances in a previous work [2] and thus selected by the authors for creating the MGC3. Since cavities are among the most interesting and valuable targets for space exploration [3][4], extending the investigated area to the whole planet could advance the state of the art and provide potential targets for future mission. Since the datasets involved are very large, with approx. products of 115,897 for CTX and 1,775,440 for HiRISE [5] a manual approach is not feasible. In this respect, computer-assisted techniques that rely mainly on Machine Learning and Deep Learning algorithms are extremely valuables, providing robust, standardized and highly customizable pipelines and tools for analysing automatically large datasets. Deep Learning Object Detection algorithms such [6] were used in this study, with proper training, can detect virtually all pit and cave entrance occurrences.

DATA AND METHODS

Data used consists of CTX and HiRISE imagery, accessed from the PDS Geosciences Node Mars Orbital Data Explorer portal and divided into train and test datasets.

Training: For training the Deep Learning Object Detection algorithm, have been used 130 HiRISE red channel images. These images have been divided into training, test, and validation sub-datasets, then the training and testing images have been scaled to approx. 1/3 of the original resolution and then tiled into 900x900 pixels image with black border removed. Then all images have been randomly flipped, rotated, and mirrored to increase the training dataset. Object labels have been created in all resulting images. The labels have been created ex-novo, according to literature description of features and feature's characteristics clearly visible in the used images Table 1. The model has been trained for approx. 24h.

Testing: validating images, have been used to check the quality of the training sessions.

Tools: All the above processing have been made using open-source tool developed in python [7][8]. YOLOv5 algorithm has been modified and integrated into Python scripts and notebooks.

LABELS

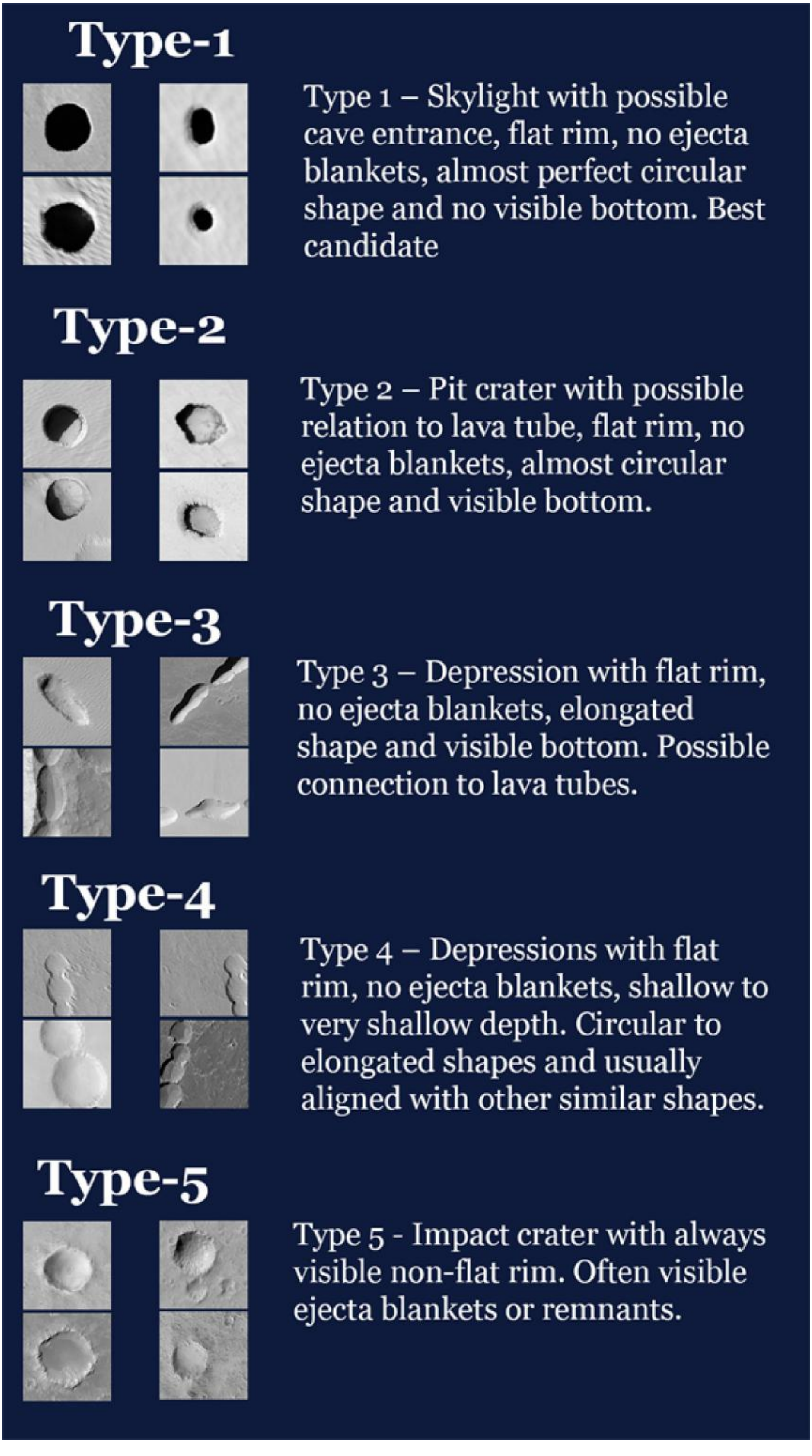

Type-1

Type 1 – Skylight with possible cave entrance, flat rim, no ejecta blankets, almost perfect circular shape and no visible bottom. Best candidate

Type-2

Type 2 – Pit crater with possible relation to lava tube, flat rim, no ejecta blankets, almost circular shape and visible bottom.

Type-3

Type 3 – Depression with flat rim, no ejecta blankets, elongated shape and visible bottom. Possible connection to lava tubes.

Type-4

Type 4 – Depressions with flat rim, no ejecta blankets, shallow to very shallow depth. Circular to elongated shapes and usually aligned with other similar shapes.

Type-5

Type 5 - Impact crater with always visible non-flat rim. Often visible ejecta blankets or remnants.

The above types have been created with the dual aim of testing the algorithm capability of discriminating similar object and integrate landforms that could potentially be the phases of the geomorphological evolution of a single landform.

TRAINING EVALUATION

Despite the small dataset used, the training has reached good results.

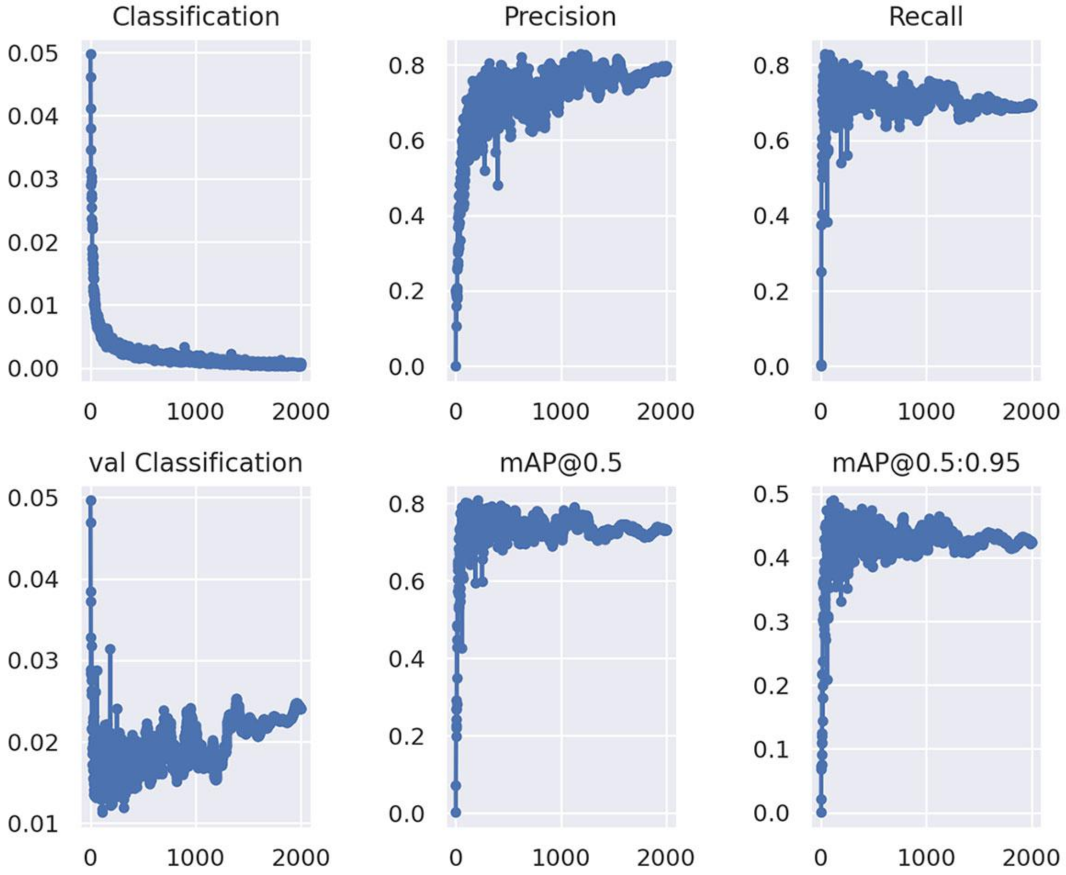

Fig. 1 - Training evaluation charts show a precision of approx 80% with a recall of 70%.

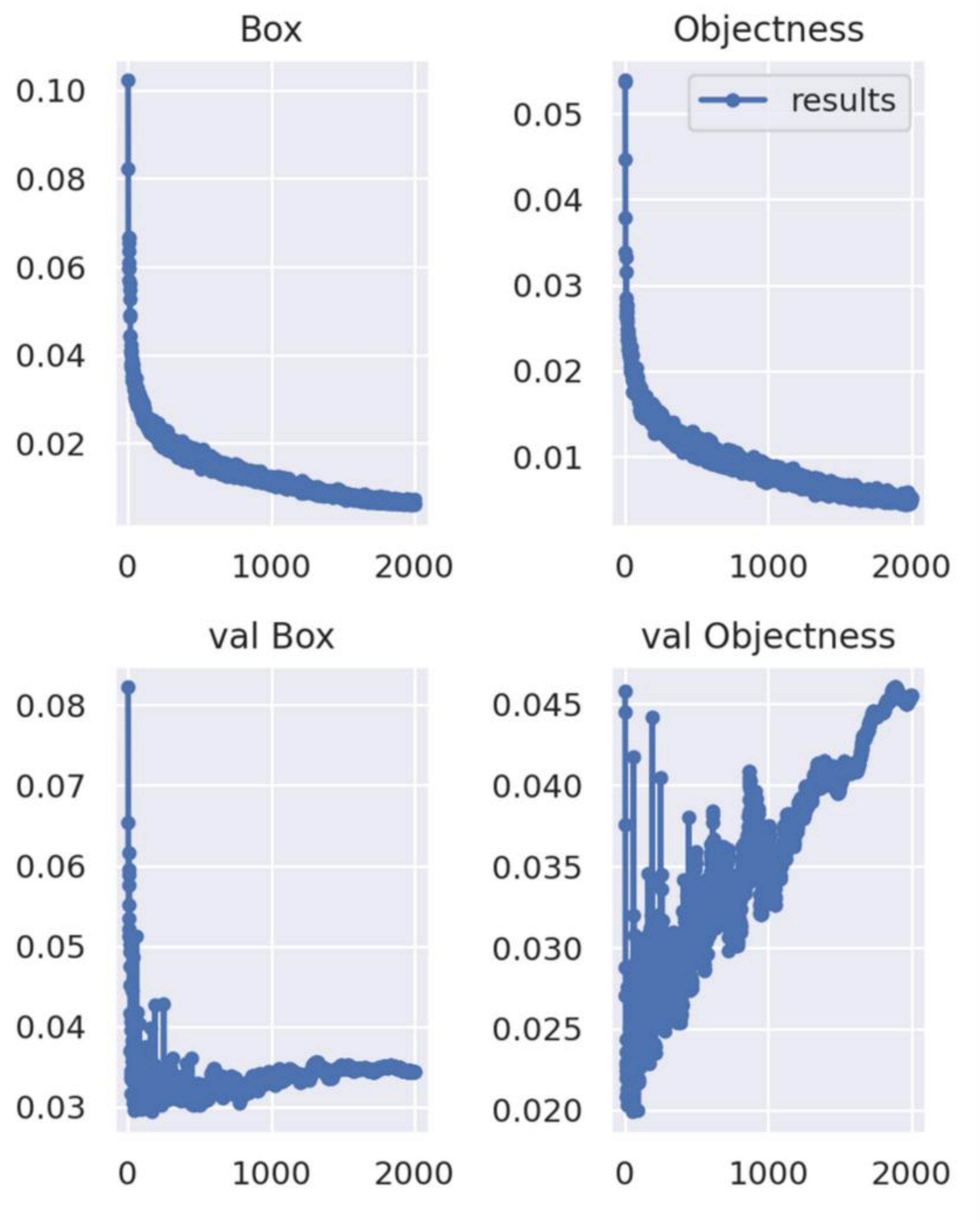

Fig. 2 - Training evaluation charts show very low loss levels.

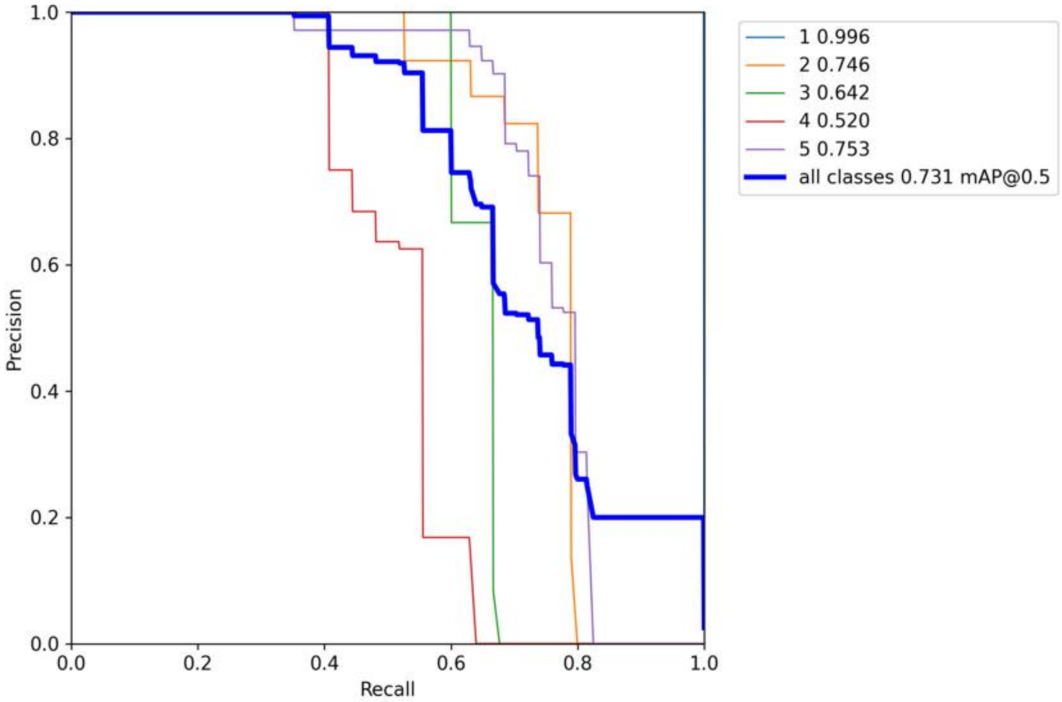

Fig. 3 - Evaluation of precision and recall parameters per each class, show a ratio near to 1 for the Type-1 class, our primary target, while the lowest scores are related to Type-3 and Type-4.

RESULTS

Trained model has been used to inference 900 HiRISE images with more than 4000 detections across all types. Even if the dataset used for this preliminary work is not the same of the one used for MGC3, there is a high correspondence between MGC^3 and the preliminary results obtained as shown in the images in the slideshow below (click on the slideshow for full images). Moreover, there are several detections of possible cave candidates (Type-1) that are not present in the MGC^3.

At this stage of work, manual validation is fundamental since there are several false positive and the training dataset is fairly small but further studies, including the increase of training dataset could lead to optimizations of the trained model and provide a reliable tool to be used to build up the MGC3 using the full datasets of HiRISE and CTX.

Furthermore, once the workflow and the developed tools are validated it will be possible to replicate this methodology to datasets of other terrestrial planets and moons.

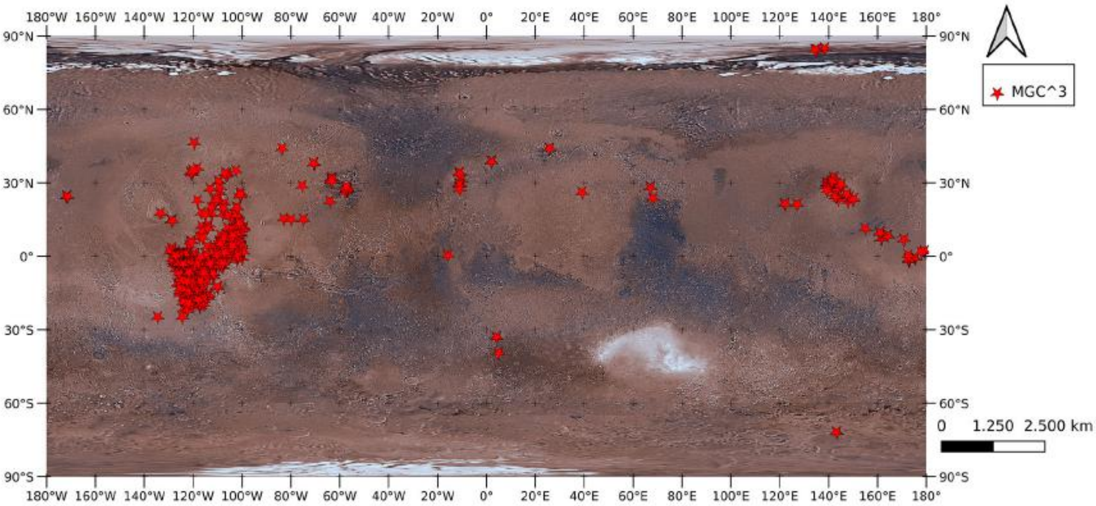

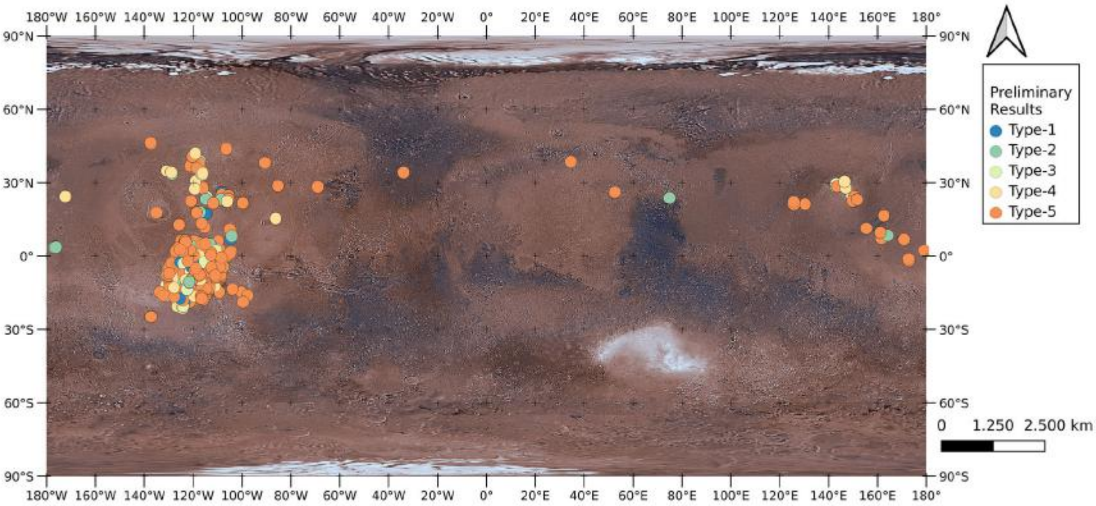

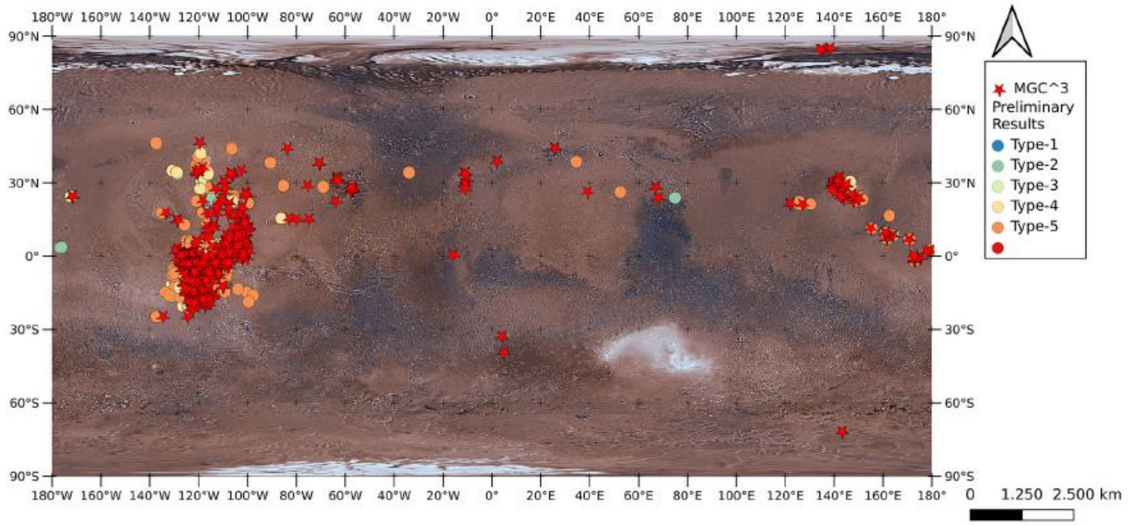
180°W 160°W 140°W 120°W 100°W 80°W 60°W 40°W 20°W 0° 20°E 40°E 60°E 80°E 100°E 120°E 140°E 160°E 180°
90°N
60°N
30°N
0°
30°S
60°S
90°S
MGC^3 Preliminary Results
Type-1
Type-2
Type-3
Type-4
Type-5
0 1.250 2.500 km

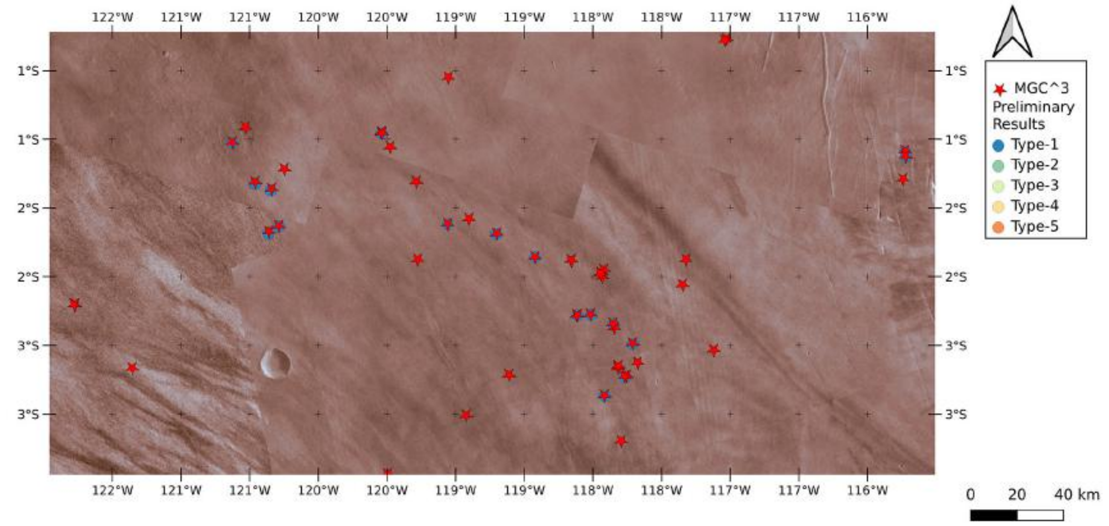
122°W 121°W 121°W 120°W 120°W 119°W 119°W 118°W 118°W 117°W 117°W 116°W
1°S
1°S
2°S
2°S
3°S
3°S
MGC^3 Preliminary Results
Type-1
Type-2
Type-3
Type-4
Type-5
0 20 40 km

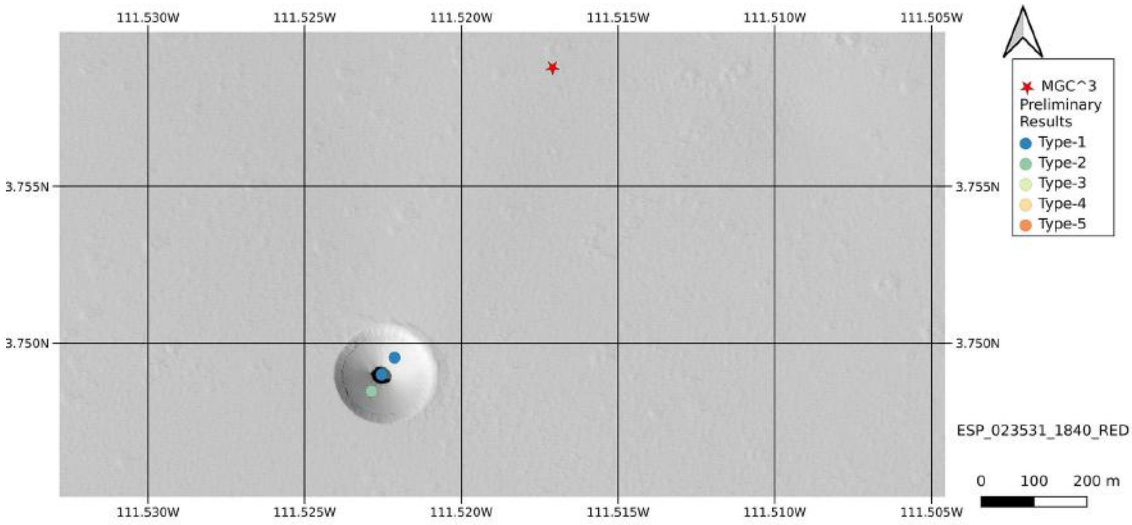
111.530W 111.525W 111.520W 111.515W 111.510W 111.505W
3.755N
3.750N
MGC^3 Preliminary Results
Type-1
Type-2
Type-3
Type-4
Type-5
ESP_023531_1840_RED
0 100 200 m

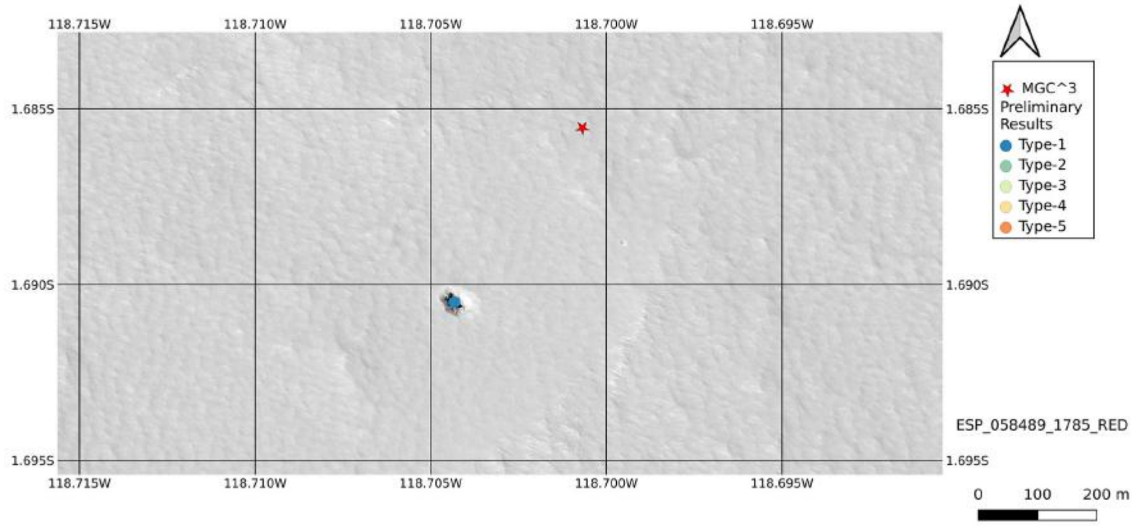
118.715W
118.710W
118.705W
118.700W
118.695W
1.685S
1.690S
1.695S
MGC^3 Preliminary Results
Type-1
Type-2
Type-3
Type-4
Type-5
ESP_058489_1785_RED
0
100
200 m

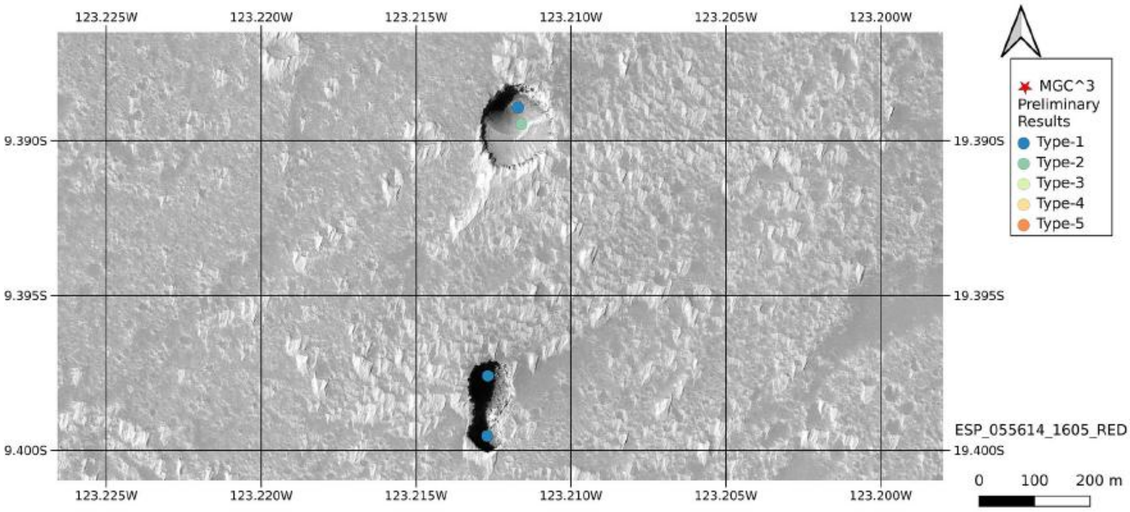
123.225W
123.220W
123.215W
123.210W
123.205W
123.200W
9.390S
9.395S
9.400S
19.390S
19.395S
19.400S
MGC^3 Preliminary Results
Type-1
Type-2
Type-3
Type-4
Type-5
ESP_055614_1605_RED
0
100
200 m

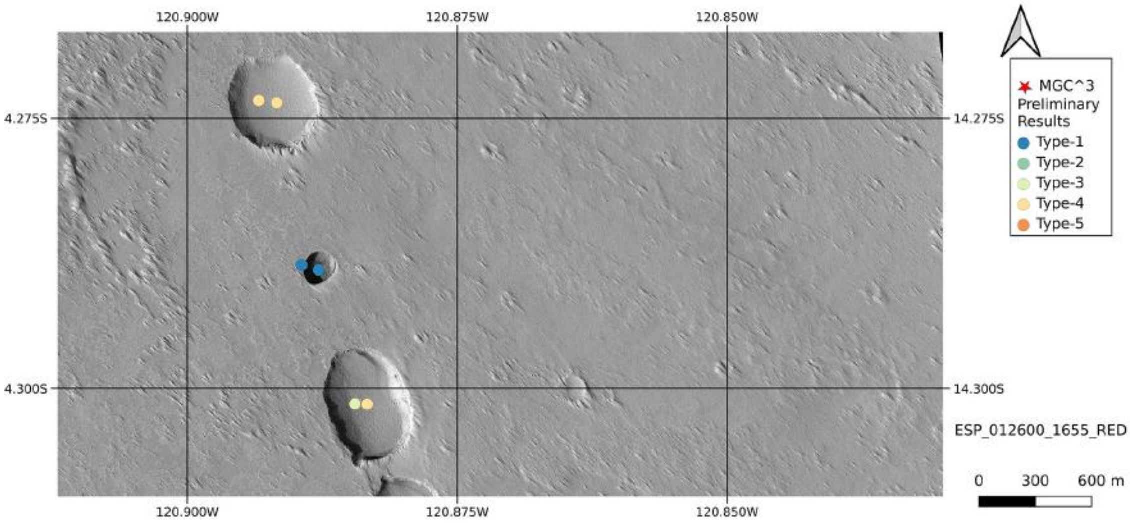
120.900W
120.875W
120.850W
4.275S
4.300S
14.275S
14.300S
MGC^3 Preliminary Results
Type-1
Type-2
Type-3
Type-4
Type-5
ESP_012600_1655_RED
0
300
600 m

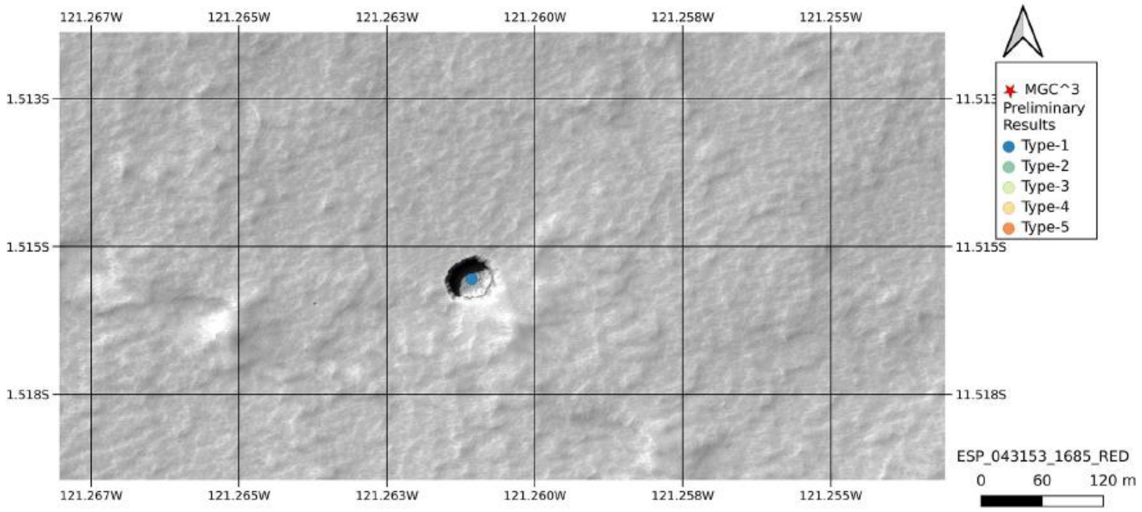
121.267W
121.265W
121.263W
121.260W
121.258W
121.255W
1.513S
1.515S
1.518S
11.513
11.515S
11.518S
MGC^3 Preliminary Results
● Type-1
● Type-2
● Type-3
● Type-4
● Type-5
ESP_043153_1685_RED
0 60 120 m

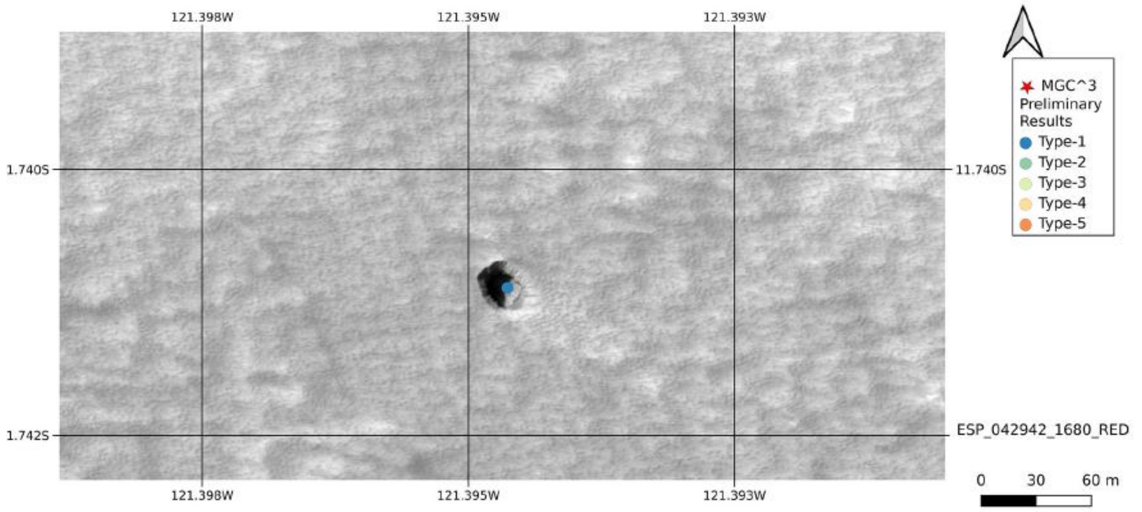
121.398W
121.395W
121.393W
1.740S
1.742S
11.740S
MGC^3 Preliminary Results
● Type-1
● Type-2
● Type-3
● Type-4
● Type-5
ESP_042942_1680_RED
0 30 60 m

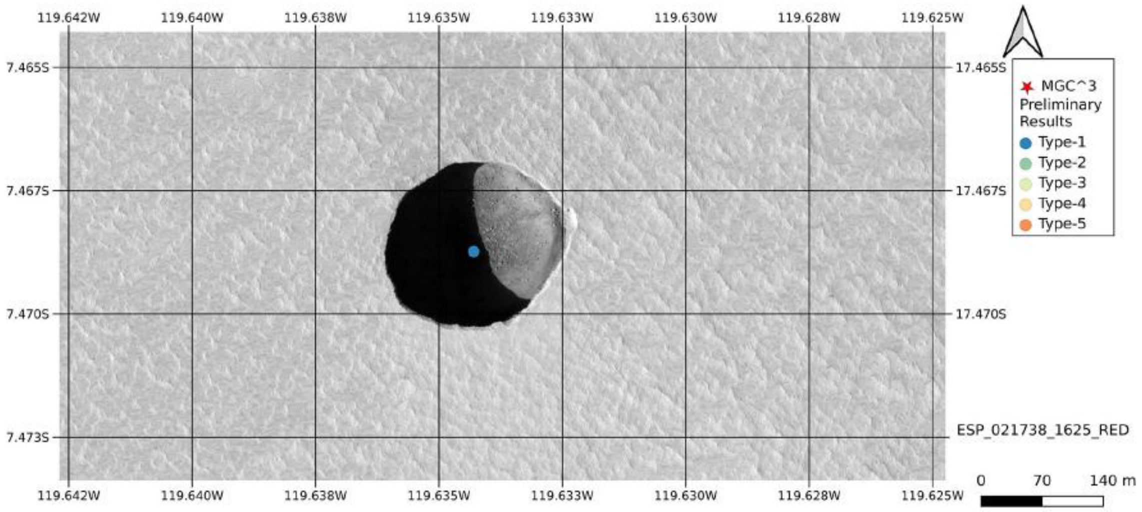
119.642W
119.640W
119.638W
119.635W
119.633W
119.630W
119.628W
119.625W
7.465S
7.467S
7.470S
7.473S
17.465S
17.467S
17.470S
MGC^3 Preliminary Results
● Type-1
● Type-2
● Type-3
● Type-4
● Type-5
ESP_021738_1625_RED
0 70 140 m

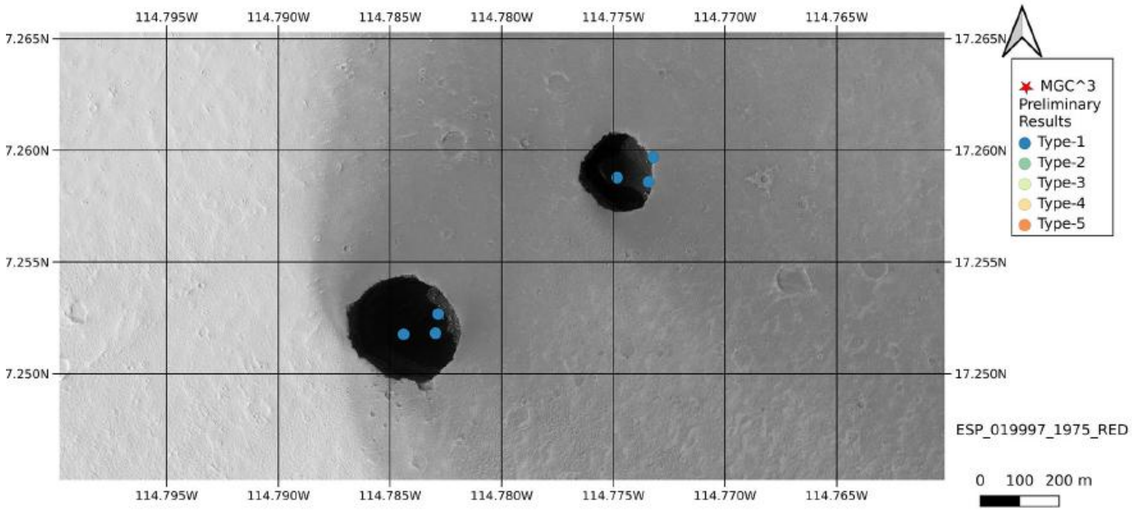
114.795W
114.790W
114.785W
114.780W
114.775W
114.770W
114.765W
7.265N
7.260N
7.255N
7.250N
17.265N
17.260N
17.255N
17.250N
MGC^3 Preliminary Results
Type-1
Type-2
Type-3
Type-4
Type-5
ESP_019997_1975_RED
0 100 200 m

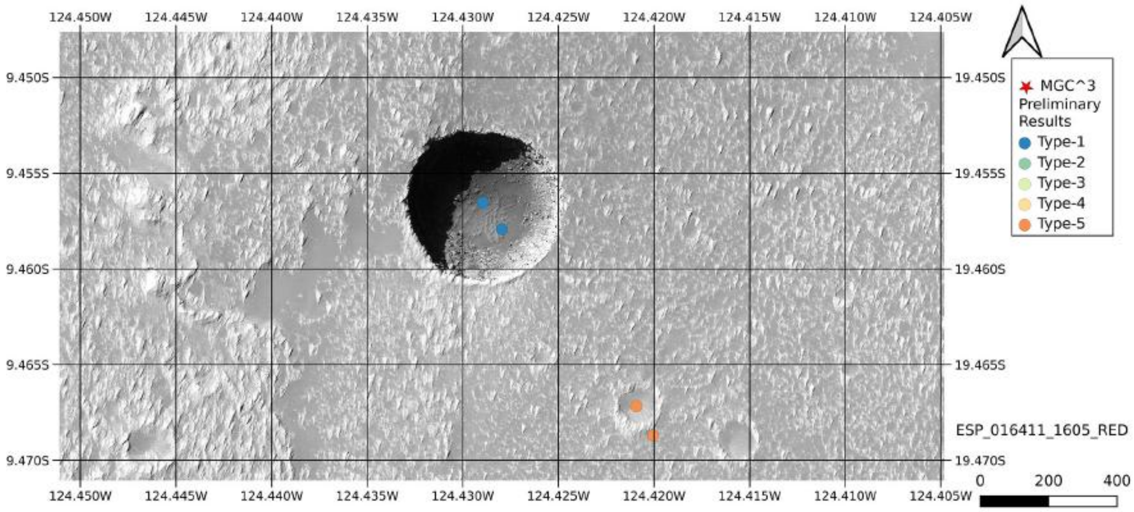
124.450W
124.445W
124.440W
124.435W
124.430W
124.425W
124.420W
124.415W
124.410W
124.405W
9.450S
9.455S
9.460S
9.465S
9.470S
19.450S
19.455S
19.460S
19.465S
19.470S
MGC^3 Preliminary Results
Type-1
Type-2
Type-3
Type-4
Type-5
ESP_016411_1605_RED
0 200 400

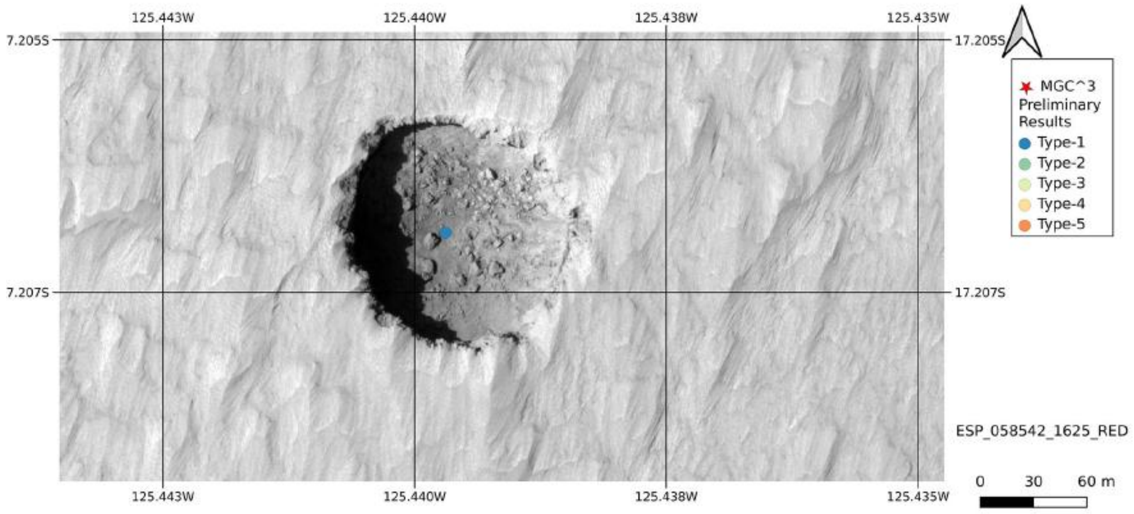
125.443W
125.440W
125.438W
125.435W
7.205S
7.207S
17.205S
17.207S
MGC^3 Preliminary Results
Type-1
Type-2
Type-3
Type-4
Type-5
ESP_058542_1625_RED
0 30 60 m

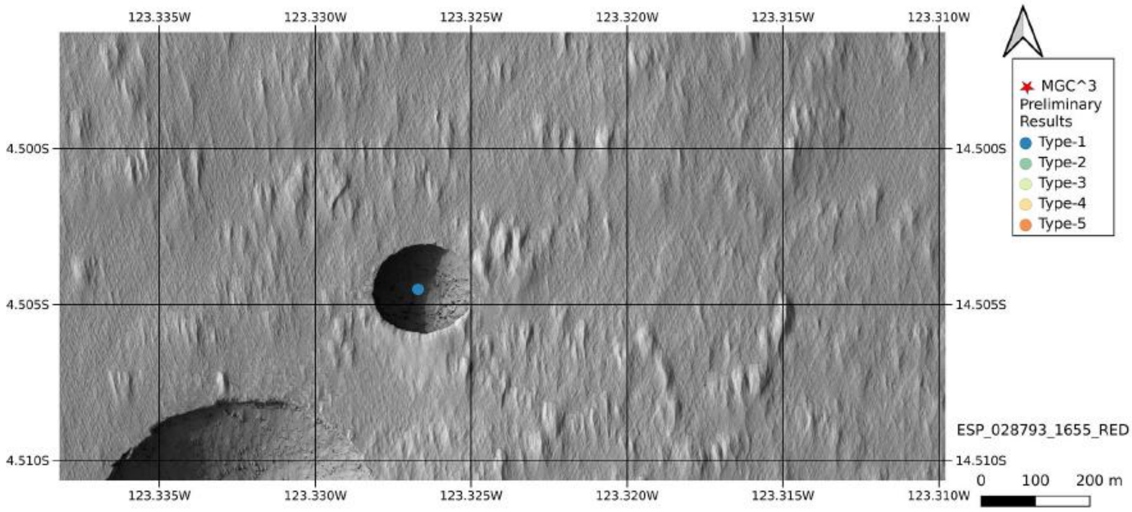
123.335W
123.330W
123.325W
123.320W
123.315W
123.310W
4.500S
4.505S
4.510S
14.500S
14.505S
14.510S
MGC^3
Preliminary
Results
Type-1
Type-2
Type-3
Type-4
Type-5
ESP_028793_1655_RED
0
100
200 m

DISCLOSURES

Acknowledgments: This study is within the Europlanet 2024 RI, and it has received funding from the European Union's Horizon 2020 research and innovation programme under grant agreement No 871149. Mars images were obtained from NASA PDS.

AUTHOR INFORMATION

g.nodjoumi@jacobs-university.de

ABSTRACT

DEEP LEARNING OBJECT DETECTION FOR MAPPING CAVE CANDIDATES ON MARS: BUILDING UP THE MARS GLOBAL CAVE CANDIDATE CATALOG (MGC^3).

G. Nodjoumi1, R. Pozzobon2, A.P. Rossi1, 1Jacobs University Bremen, Bremen, Germany, g.nodjoumi@jacobs-university.de; 2Department of Geosciences, University of Padova, Padova, Italy

Introduction: The Mars Global Cave Candidate Catalog (MGC3) v1, published by Cushing et al. [1] in 2017 contains the locations and a short description of more than 1000 possible cave-entrances on Mars that have been identified by manually surveying images acquired by Mars Odyssey's (MO) Thermal Emission Imaging System (THEMIS) and Mars Reconnaissance Orbiter's (MRO) Context Camera (CTX) and High Resolution Imaging Science Experiment (HiRISE) cameras. Authors analysed all images that covers the area north of Arsia Mons (235° to 243° E, 28° to 2° N). The Arsia Mons is a shield volcano, located in the southern area of the large Tharsis Region, on whose flanks have been identified at least 7 possible cave entrances in a previous work [2] and thus selected by the authors for creating the MGC3. Since cavities are among the most interesting and valuable targets for space exploration [3][4], extending the investigated area to the whole planet could advance the state of the art and provide potential targets for future mission. Since the datasets involved are very large, with approx. products of 115,897 for CTX and 1,775,440 for HiRISE [5] a manual approach is not feasible. In this respect, computer-assisted techniques that rely mainly on Machine Learning and Deep Learning algorithms are extremely valuables, providing robust, standardized and highly customizable pipelines and tools for analysing automatically large datasets. Deep Learning Object Detection algorithms such [6] were used in this study, with proper training, can detect virtually all pit and cave entrance occurrences.

Data and Methods: Data used consists of CTX and HiRISE imagery, accessed from the PDS Geosciences Node Mars Orbital Data Explorer portal and divided into train and test datasets.

Training: For training the Deep Learning Object Detection algorithm, have been used 130 HiRISE red channel images. These images have been divided into training, test, and validation sub-datasets, then the training and testing images have been scaled to approx. 1/3 of the original resolution and then tiled into 900x900 pixels image with black border removed. Then all images have been randomly flipped, rotated, and mirrored to increase the training dataset. Object labels have been created in all resulting images. The labels have been created ex-novo, according to literature description of features and feature's characteristics clearly visible in the used images Table 1. The model has been trained for approx. 24h.

Image	ID	Description
	1	Type 1 – Skylight with possible cave entrance, flat rim, no ejecta blankets, almost perfect circular shape and no visible bottom. Best candidate
	2	Type 2 – Pit crater with possible relation to lava tube, flat rim, no ejecta blankets, almost circular shape and visible bottom.
	3	Type 3 – Depression with flat rim, no ejecta blankets, elongated shape and visible bottom. Possible connection to lava tubes.
	4	Type 4 – Depressions with flat rim, no ejecta blankets, shallow to very shallow depth. Circular to elongated shapes and usually aligned with other similar shapes. May be related to lava tube collapse [4], secondary impacts or geomorphological evolution of other types due to other processes such wind erosion.
	5	Type 5 - Impact crater with always visible non-flat rim. Often visible ejecta blankets or remnants.

Table 1 – Classes used for label training dataset.

Testing: validating images, have been used to check the quality of the training sessions.

Tools: All the above processing have been made using open-source tool developed in python [7][8]. YOLOv5 algorithm has been modified and integrated into Python scripts and notebooks.

Results: Trained model has been used to inference 900 HiRISE images and 50 CTX images mainly of Tharsis region. Detection have been georeferenced, and a shapefile has been created. In figure 1 is shown an example of HiRISE image (with bounding boxes of detected objects. For each box is shown the ID of the detection and a confidence score (0 to 1). In figure 2 is shown a comparison between MGC3and results of the inference in the Tharsis region. Even if the dataset used for the test is not the same of the one used for MGC3, there is a high correspondence between MGC3and obtained results as shown in Figure 2 and Figure 3.

Figure 1 - Example of detections obtained on HiRISE images. For each detection, the first number represent the type and the second represent the confidence level.

Figure 2 - Comparison between MGC3 and obtained results over Tharsis Region.

Figure 3 - Detail of comparison between MGC3 and obtained results on HiRISE ESP_023523_3840_RED.

The most promising results are potential new detections not present in the MGC3, that still needs to be manually validated (Figure 4).

Figure 4 - Example of possible new cave candidate on HiRISE ESP_028793_1655_RED.

Conclusions: Preliminary results obtained using a Deep Learning object detection algorithm provided promising results, since there are: a high correspondence with the MGC3 candidates, new detections of cave candidates and detections of craters. At this stage of work, manual validation is fundamental since there are several false positive and the training dataset is fairly small but further studies, including the increase of training dataset could lead to optimizations of the trained model and provide a reliable tool to be used to build up the MGC3 using the full datasets of HiRISE and CTX.

Acknowledgments: This study is within the Europlanet 2024 RI, and it has received funding from the European Union’s Horizon 2020 research and innovation programme under grant agreement No 871149. Mars images were obtained from NASA PDS.

References: [1] Cushing G.E. (2017) Mars Global Cave Candidate Catalog (MGC3). [2] Cushing et al. (2007) Themis observes possible cave skylights on Mars. [3] Cushing G.E. (2012) Candidate cave entrances on Mars. [4] Sauro R. et al. (2020) Lava tubes on Earth, Moon and Mars: A review on their size and morphology revealed. [5] PDS Geosciences Node Orbital Data Explorer (ODE). [6] Redmon J. et al. (2016) You Only Look Once: Unified, Real-Time Object Detection. [7] Nodjoumi G. (2020) ImageProcessingUtils (https://zenodo.org/record/4396191). [8] Nodjoumi G. (2020) DeepLandforms-YOLOv5 (http://doi.org/10.5281/zenodo.4430015)

REFERENCES

[1] Cushing G.E. (2017) Mars Global Cave Candidate Catalog (MGC3).

[2] Cushing et al. (2007) Themis observes possible cave skylights on Mars.

[3] Cushing G.E. (2012) Candidate cave entrances on Mars.

[4] Sauro R. et al. (2020) Lava tubes on Earth, Moon and Mars: A review on their size and morphology revealed.

[5] PDS Geosciences Node Orbital Data Explorer (ODE).

[6] Redmon J. et al. (2016) You Only Look Once: Unified, Real-Time Object Detection.

[7] Nodjoumi G. (2020) ImageProcessingUtils (https://zenodo.org/record/4396191).

[8] Nodjoumi G. (2020) DeepLandforms-YOLOv5 (http://doi.org/10.5281/zenodo.4430015)